Dynamic FE simulation of four-story steel frame modeled by solid elements and its validation using results of full-scale shake-table test

AUTHOR(S):

Miyamura, Tomoshi; Yamashita, Takuzo; Akiba, Hiroshi; Ohsaki, Makoto

Submitted to EARTHQUAKE ENGINEERING & STRUCTURAL DYNAMICS (Preprint)

Dynamic FE Simulation of Four-story Steel Frame Modeled by Solid Elements and Its Validation Using Results of Full-scale Shake-table Test

Tomoshi Miyamura*,**, Takuzo Yamashita**, Hiroshi Akiba***, Makoto Ohsaki****

* Corresponding author.
Department of Computer Science, College of Engineering, Nihon University
1 Nakagawara, Tokusada, Tamura, Koriyama 963-8642, Japan
(Hyogo Earthquake Engineering Research Center, National Research Institute for Earth Science and Disaster Prevention)
Phone: +81-24-956-8829, Fax: +81-24-956-8863, miyamura@cs.ce.nihon-u.ac.jp

** Hyogo Earthquake Engineering Research Center, National Research Institute for Earth Science and Disaster Prevention
1501-21 Nishikameyama, Mitsuta, Shijimi, Miki 673-0515, Japan, tyamashi@bosai.go.jp

*** Allied Engineering Corporation
Toyosu Front, 3-2-20 Toyosu, Koto-ku, Tokyo 135-0061, Japan, akiba@alde.co.jp

**** Department of Architecture, Hiroshima University
1-4-1 Kagamiyama, Higashi-Hiroshima 739-8527, Japan, ohsaki@hiroshima-u.ac.jp

Keywords: Steel Building Frame, Seismic Response, Collapse, Parallel Finite Element Analysis, Full-scale Shake-table Test, Validation

Running Head: **FE Simulation of Four-story Steel Frame Modeled by Solid Elements**

Abstract: Dynamic finite element analyses of a four-story steel building frame modeled as a fine mesh of solid elements are performed using E-Simulator, which is a parallel finite element analysis software package for precisely simulating collapse behaviors of civil and building structures. E-Simulator is under development at the National Research Institute for Earth Science and Disaster Prevention (NIED), Japan. A full-scale shake-table test for a four-story frame was conducted using E-Defense at NIED, which is the largest shaking table in the world. A mesh of the entire structure of a four-story frame with approximately 19 million degrees of freedom is constructed using solid elements. The density of the mesh is determined by referring to the results of elastic-plastic buckling analyses of a column of the frame using meshes of different densities. Therefore, the analysis model of the frame is well verified. Seismic response analyses under 60%, 100%, and 115% excitations of the JR Takatori record of the 1995 Hyogoken-Nanbu earthquake are performed. Note that the simulation does not reproduce the collapse under the 100% excitation of the Takatori record in the E-Defense test. Therefore, simulations for the 115% case are also performed. The results obtained by E-Simulator are compared with those obtained by the E-Defense full-scale test in order to validate the results obtained by E-Simulator. The shear forces and interstory drift angles of the first story obtained by the simulation and the test are in good agreement. Both the response of the entire frame and the local deformation due to elastic-plastic buckling are simulated simultaneously using E-Simulator.

1. Introduction

A 3-D full-scale earthquake testing facility, E-Defense, which has the largest shaking table in the world, is located at the Hyogo Earthquake Engineering Research Center of the National Research Institute for Earth Science and Disaster Prevention (NIED), Japan [1] [2]. One reason for conducting shake-table tests using E-Defense is to validate simulation codes. In NIED, a parallel finite element software package, E-Simulator, is under development for precisely simulating collapse behaviors of civil and building structures subjected to earthquakes [3]. The platform of E-Simulator is a general-purpose parallel finite element analysis code, ADVENTURECluster [4]-[7], which is a commercial version of the ADVENTURE system, an open-source parallel CAE software package [8][9]. ADVENTURECluster uses the framework of the ADVENTURE system and is equipped with a linear solver that was developed by one of the authors and various extended functions, as described in Section 2. These codes enable large-scale finite element analyses to be performed using meshes with 10 to 100 million degrees of freedom. E-Simulator inherits this ability to perform large-scale parallel computations, and both the global behavior and local behaviors, such as buckling and fracture of a material, are simulated simultaneously using a very fine mesh of solid elements. Note that conventional commercial finite element analysis codes cannot solve problems with more than 10 million degrees of freedom, which limits the use of a sufficiently fine mesh to capture local phenomena. Dynamic collapse analyses of steel frames using a fine mesh of solid elements have been conducted using E-Simulator [10], [11].

In the field of building engineering, beam element models and macro-models, such as plastic hinge models and fiber element models, have been widely used. Numerical simulations using two-dimensional frame models have been conducted for steel frames, and these simulations still have important roles in designing and analyzing building frames [12]-[15]. Recently, three-dimensional frame models [16]-[23] have been widely used. These models are classified as concentrated models, in which inelasticity is concentrated at the ends of a member, and distributed models, in which inelasticity is distributed along the length of the member. A beam element based on the finite element method is classified as belonging to the latter type. The model in Ref. [21] has characteristics of both types. The distributions of stresses and inelasticity in a cross section can be considered using a fiber-based approach. In the macro-models, the local buckling of the member is usually taken into account using a particular material model. However, it may be difficult to develop a macro-model that covers all possible complex buckling behaviors under combined loadings of the two-directional bending and fluctuated axial load.

A detailed finite element model of shell elements is used for the simulation of steel frames [17], [18], [24]. One advantage of a solid element over a shell element is that general constitutive equations for a three-dimensional state can be used. On the other hand, the assumption of the plane stress state is introduced in a standard shell element, and special treatments are necessary in order to develop its constitutive equation. Moreover, the mesh density in the in-plane directions for an analysis model with shell elements should be equivalent to that for an analysis model with solid elements. Therefore, the total number of degrees of freedom for the model with solid elements is less than twice that for the model with shell elements, if the plates of steel members are discretized into two layers of solid elements.

A full-scale shake-table test for a four-story steel frame (Figure 1) was conducted using E-Defense [25][26]. A blind analysis contest was held along with the test [27]. Tada et al. [17], [18] conducted three-dimensional analyses of the four-story frame and compared the results with those obtained by the E-Defense test. They developed a collaborative structural analysis

(CSA) system in which several structural analysis programs are integrated via the Internet. A structure is divided into several substructures, and each substructure is simulated using an individual program. The local buckling of a column is analyzed using a mesh of shell elements. Nam and Kasai [19] conducted 3D analyses of the four-story frame using a fiber element method in which the effect of local buckling at the column ends is taken into account. They also investigated the effect of exterior walls on the strength and stiffness of the entire frame. The present authors [11] performed a preliminarily simulation of the test of the four-story frame using E-Simulator. Isobe et al. [20] performed analyses of the frame using an adaptive finite element code, the ASI-Gauss code [21]. The ASI-Gauss method is based on the linear Timoshenko beam element. They compared the results with those obtained by E-Simulator [11] and the experimental results of the E-Defense test in order to verify and validate (V&V) their code. Lignos et al. [15] analyzed the sidesway collapse of another four-story steel frame using a two-dimensional frame model. They conducted a number of component tests in order to configure plastic hinges. Wang et al. [16] conducted a distributed online hybrid test for a four-story steel frame having dimensions that are different from but similar to those of the four-story frame examined in the E-Defense test. They tested a two-dimensional middle planar frame. The superstructure in the hybrid test is simulated using a beam and plastic hinge model in a commercial finite element analysis code. They simulated the collapse behavior of the frame.

In the present study, seismic response analyses of the four-story steel frame using E-Simulator under the 60%, 100%, and 115% excitations of the JR (Japan Railway) Takatori record of the 1995 Hyogoken-Nanbu earthquake are performed. Note that the simulation does not reproduce the collapse under the 100% excitation of the Takatori record in the E-Defense test. Therefore, simulations for the 115% case are also performed. E-Simulator is validated by comparing its results with experimental results obtained by the full-scale shake-table test conducted using E-Defense. The analysis model used in the previous study [11] is improved from the viewpoints of precise geometry modeling and material modeling. The advantages of an analysis model that uses a very fine mesh of solid elements are demonstrated by showing that both global behaviors, such as the collapse of the frame, and local behaviors, such as the local buckling of columns, are simulated simultaneously and precisely.

The remainder of the present paper is organized as follows. In Section 2, an overview of E-Simulator is presented. Section 3 describes the verification of an analysis model for a column of a four-story frame. Static elastic-plastic buckling analysis under a lateral prescribed displacement is performed for meshes with different mesh densities. Then, a mesh of the four-story frame that is made of solid elements is shown. In Section 4, the results of the numerical simulation of the four-story frame are presented. Concluding remarks are presented in Section 5.

2. E-SIMULATOR

2.1 Purpose

E-Simulator is a parallel implicit finite element structural analysis code for virtual shake-table tests of civil and building structures that enables large-scale analysis to be performed with a very fine mesh of solid elements. In conventional analysis methods for steel building frames, empirically defined macro-models, such as plastic hinge models and fiber models, are often used. The results of analyses using such macro-models depend on the assumptions included in the models. The macro-models represent mechanical behaviors of structural components. Therefore, an experimental evaluation of the structural component is necessary in order to determine the appropriate model parameters for a macro-model. Numerous component tests are necessary for components of different sizes. On the other hand,

E-Simulator enables large-scale structural analysis to be performed with a very fine mesh of solid elements. In this case, only simple material tests are necessary in order to determine the material properties for the constitutive equations used in the solid element. Although tests for structural components must be carried out in order to validate the analysis code and analysis model, the number of tests required can be reduced.

2.2 Overview

The main core of E-Simulator is the commercial software package ADVENTURECluster [4]-[7], which has been extended from the open-source version, the ADVENTURE system [8], [9]. These packages use the domain decomposition method in the linear algebraic solver and in parallel implementation. The structural analysis code, ADVENTURE_Solid in the ADVENTURE system, adopts the balancing domain decomposition (BDD) method [28], which is a substructuring-based linear iterative method with a Neumann-Neumann preconditioner combined with coarse grid correction. On the other hand, Akiba et al. [5], [7] originally developed the Coarse Grid Conjugate Gradient (CGCG) method for ADVENTURECluster. The CGCG method is an iterative method with a coarse grid correction that is similar to that used in the BDD method. However, it is not a substructuring-based iterative method, and the computation cost for static condensation in each subdomain is reduced. ADVENTURECluster uses the same framework as ADVENTURE_Solid, i.e., the hierarchical domain decomposition method (HDDM) [29]. In the HDDM, two-level domain decomposition is adopted. The mesh is first subdivided into subdomains called Parts, and then each Part is subdivided into subdomains. In ADVENTURE_Solid, all input data are generalized and divided hierarchically into Part data or subdomain data [30]. A similar generalized data format is also adopted in ADVENTURECluster/E-Simulator. ADVENTURECluster can be operated in a massively parallel computational environment. ADVENTURECluster was implemented on Blue Gene/L in 2006, and the research was selected as a finalist for the 2006 Gordon Bell Prize [6].

In ADVENTURECluster, basic functions that are necessary for a general-purpose finite element code are implemented. For implicit dynamic analysis, the Hilber-Hughes-Taylor time integration method (α-method) [31] is implemented. In the following analyses, the parameter α in the scheme for introducing numerical damping is taken to be -0.05. Various finite elements are prepared. Standard inelastic constitutive equations are implemented. In E-Simulator, inelastic constitutive equations and rupture/fracture models that are particular to civil and building structures are implemented as an extended function. For example, a constitutive model with a piecewise-linear combined isotropic-kinematic hardening model [32] is implemented for accurately modeling the rolled mild steel material. This material model is based on the von Mises yield criterion using a combined isotropic-kinematic hardening rule with a number of piecewise-linear hardening curves. Implicit and heuristic rules are introduced to represent the yield plateau, the Bauschinger effect, and the hardening properties in cyclic loading. The constitutive equation is described in detail in Reference [32]. Material models of concrete and soil are also implemented in E-Simulator.

One of the important functions in structural analyses is the imposition of multi-point constraints (MPCs). The incorporation of MPCs into domain decomposition methods is a challenging area of research, especially when the number of imposed MPCs is very large. The CGCG method is applied to a projective space (see for example Reference [33]) represented by a constraint matrix of MPCs, and several million MPCs can be taken into account. A rigid beam element that connects both translational and rotational degrees of freedom is also implemented using a set of MPCs. The rigid body element has six degrees of freedom in each node, i.e., three translational degrees of freedom and three rotational degrees of freedom. An

arbitrarily shaped rigid body is represented by a number of rigid beam elements. A point load or a prescribed displacement can be applied at a node of rigid beam elements. Numerous MPCs and rigid body elements are used in the model of the four-story steel frame introduced in the following section.

3. Fine mesh of solid elements for a four-story steel frame

A finite element mesh that consists of hexahedral solid elements is generated for the four-story steel frame, as shown in Figure 1. Before generating the mesh of the entire structure, meshes of a column of the structure with different mesh densities are generated, and the elastic-plastic buckling analyses of the column are conducted using the meshes for the calculation verification of the analysis model. Then, the mesh density of each part of the four-story frame is determined.

3.1 Verification of the analysis model using solid elements

Both global and local behaviors can be simulated using a fine mesh of solid elements. A typical local behavior of a steel frame is the elastic-plastic local buckling of each member. The finite element mesh should be fine enough to reproduce the deformation due to the buckling. Yamashita et al. [34] conducted static finite element elastic-plastic buckling analyses of a square steel tube column subjected to increasing lateral displacement using meshes of different densities in order to verify the analysis model. In this section, some results of this research that are related to the four-story frame are briefly introduced.

The column corresponds to the C1 column of the four-story frame. The column is located at the intersection of line A and line 2 and is indicated in red in Figure 1. Figure 2 shows a typical finite element mesh of the column of a square tube. The number of divisions in the lateral directions (directions along each edge of the cross section) is represented by n. The number of divisions in the thickness direction and that in the z-direction (longitudinal direction) are represented by m and k, respectively. Then, the mesh of the column is represented by *tmbnLk*. The mesh in Figure 2 shows the model *t*2*b*12*L*80. The lower end of the column is fixed. An additional control node is placed at the center of the upper end of the column. Each node in the upper end is connected to the control node using a rigid beam element. The control node is fixed in the x-direction and is free in the z-direction. The rotational degree of freedom around the x-axis is fixed, i.e., the rotation of the rigid beams is fixed. A monotonically increasing history of displacement is prescribed in the y-direction. No geometric imperfections are imposed on the present analysis model. Note that the local buckling of interest here is not triggered by an imperfection, but rather is triggered by the deformation just before the buckling occurs.

The total mass of the second floor, including the slab, nonstructural components, and so on, is 2.067×10^5 kg, and the C1 column is assumed to support one fourth of the mass, i.e., 5.169×10^4 kg. The piecewise-linear isotropic hardening model is used for steel, and its parameters are determined from the uniaxial test results distributed for the blind analysis contest [27].

Figure 3 shows a typical deformation due to the elastic-plastic local buckling. The buckling in an inextensible mode is observed. Note that the hexahedral element using linear interpolation functions enhanced by incompatible modes [35][36] is used in the analysis. The element is fully integrated using eight integration points. The deformation shown in Figure 3 cannot be simulated using the conventional linear hexahedral element without the incompatible modes. Figure 4 shows the relationship between the prescribed displacement and the reaction force in the y-direction at the loading point. The solid line indicates the solution obtained using a very fine mesh, i.e., Model *t*8*b*48*L*320. The hexahedral element

enhanced by the incompatible modes is used. This solution is shown as the reference solution in the following figures. The dotted line indicates the solution obtained using the fully integrated linear hexahedral elements without the incompatible modes. The element with the incompatible modes is used in the following analyses.

Figure 5 shows the relationships between the prescribed displacement and the reaction force for different mesh divisions in the lateral directions and in the longitudinal direction. The following aspect ratios are also shown in the figures:

$$r_b = \min\left\{b_e / L_e, L_e / b_e\right\} \quad (1)$$

$$r_t = \min\left\{t_e / L_e, L_e / t_e\right\} \quad (2)$$

where b_e, t_e, and L_e are the sizes of the element in the b (lateral), the t (thickness), and the L (longitudinal) directions, respectively.

Figure 5(a) suggests that the fine division in the longitudinal direction contributes to the improvement of the solution. On the other hand, Figure 5(b) shows that the improvement of the solution due to the fine division in the lateral directions is small. The effect of the fine division in the thickness direction is shown in Figure 6. Three different numbers of divisions in the thickness direction, i.e., 2, 4, and 8, are compared for models $b12L80$, $b24L160$, and $b48L320$, which have the same aspect ratio r_b. Figure 6(a) shows that model $b12L80$ cannot represent the accurate solution even when the number of divisions in the thickness direction is 8. In the case of model $b24L160$, the solution improves by increasing the number of divisions in the thickness direction, as shown in Figure 6(b). Figure 6(c) shows that an accurate solution can be obtained even when the number of divisions in the thickness direction is two, so long as the number of divisions in the lateral and longitudinal directions is sufficiently large. Note that the number of CG iterative steps of the CGCG method increases when the aspect ratios r_b and r_t are small and the computation time is also increased. The accuracy and computation time of the analysis depend not only on the number of mesh divisions but also on the aspect ratio of each finite element. Note that the current version of the CGCG method is not equipped with any particular preconditioning method for meshes with elements having a very small aspect ratio.

The analyses are also conducted using meshes in which the division in the longitudinal direction is fine in the regions around the two ends of the column at which buckling occurs, and is coarser in other regions. An accurate solution is obtained using these meshes. Although the number of CG iterative steps is increased due to the small aspect ratio in the coarse mesh region, the total computation time for these models is reduced compared to the model of the homogeneously fine mesh because the total number of degrees of freedom is reduced.

Next, dynamic elastic-plastic buckling analyses are performed for different meshes and different time increments in order to investigate the effect of the amplitude of the time increment. The time history of the acceleration in the y-direction is prescribed on the lower end surface of the same column as in the static case. A periodic input wave of the acceleration represented by a sine function having a frequency of 0.8 Hz and a maximum amplitude of 4 m/s^2 is applied. The amplitude increases gradually from 0 s to 5 s. The displacements in the x- and z-directions on the lower end surface are constrained. A mass of 5.169×10^4 kg, which represents the mass supported by the C1 column, is placed at the additional control node that is defined at the center of the upper surface using rigid beam elements. ADVENTURECluster/E-Simulator has the function of automatic adaptation of the time increment Δt. The lower limit of the width of the time increment is set as 2.0×10^{-4} s. The initial time increment that is also used as an upper limit is denoted by Δt_0.

Figure 7 shows the time history of the displacement in the y-direction at the center of the

upper surface for different initial time increments Δt_0 and for meshes with different mesh divisions. Figure 8 shows the time increment in each step for each model. In Table 1, the numbers of time steps for different cases are compared. Although the time increment is reduced automatically when buckling occurs in order to improve the convergence of the Newton-Raphson method, the total number of time steps is reduced for the cases with Δt_0 = 0.04. As shown in Figure 7, in the case of a fine mesh, i.e., model *t*2*b*48*L*320, approximately the same results are obtained for Δt_0 = 0.01s and 0.04s. On the other hand, the results are different for Δt_0 = 0.01s and 0.04s in the case of model *t*2*b*12*L*80. In this case, the result for the time history of the displacement with $\Delta t_0 = 0.04$ s is similar to that for model *t*2*b*48*L*320. However, this is only a coincidence. The deformation and distribution of the stress obtained by model *t*2*b*12*L*80 with Δt_0 = 0.04s is very different from those obtained by model *t*2*b*48*L*320. For the dynamic buckling problem, which is a kind of slow dynamics problem, accurate results can be obtained using a fine mesh, but with a rather large time increment.

3.2 Finite element mesh of the four-story frame

The mesh of the four-story frame in Figure 1 using hexahedral elements, as shown in Figure 9, is generated by referring to the results shown in the previous section. The finite element mesh that was generated in the Noguchi Laboratory at Keio University, Japan, is used as a prototype of the mesh. The original mesh is modified using the 3D-CAD software, I-DEAS, which has functions for generating a hexahedral mesh. A list of the members and the dead load distribution can be found in Ref. [20]. The final mesh has 4,532,742 elements, 6,330,752 nodes, and 18,992,256 DOFs. Plates used for rectangular tube columns and flanges and webs of beams are divided into at least two layers of solid elements in the thickness direction (Figure 9(b)). Plates are divided into three layers at the region in which plates of different thicknesses are connected. The size of each element in the longitudinal direction of a beam or a column is approximately 13 mm near the connections, where severe plastic deformation is expected, while a coarser mesh is used for elements located far from the connections. In Figure 10 and Table 2, the mesh of the column of the four-story frame model and the mesh of model *t*2*b*48*L*320 are compared. The number of divisions in the thickness direction for the mesh of the column is two. As shown in Figure 6(c), the solution obtained using model *t*2*b*48*L*320 approximately agrees with the reference solution obtained using model *t*8*b*48*L*320. The mesh division in the lateral directions for the column of the four-story frame model is not homogeneous so that the column can be connected to other members such as H-shaped beams without using MPCs but rather by consistently sharing nodes of different members. Although the mesh division in the lateral directions is coarser than that of the reference mesh of model *t*8*b*48*L*320, the division in the longitudinal direction is fine enough for our present needs. The same problem as shown in Figures 3 and 4 is solved using the mesh of the column in Figure 10(a), and the relationship between the prescribed displacement and the reaction force in the *y*-direction at the loading point is compared with the reference solution in Figure 11. The two curves are in approximate agreement, and the mesh in Figure 10(a) is determined to be reasonable. In Table 3, the minimum and maximum values of the aspect ratio that is defined as $\min\{r_b, r_t\}$ with r_b and r_t taken from Equations (1) and (2), respectively, and the minimum and maximum lengths of the edges of the elements are shown for each story of the frame.

Each floor slab is also divided into solid elements with two layers in the thickness direction. According to the component tests conducted by Yamada et al. [37], the slab and column come into contact, influencing the response under cyclic loading. However, the

computation cost of the dynamic contact problem is high for the current version of ADVENTURECluster/E-Simulator. Therefore, simulations are conducted only for the cases with the stick condition (in which two surfaces are always in contact and no sliding occurs) and the condition without any contact (separate condition), and the results of these two cases are compared. The regions in which the contact between the slab and the column occurs are shown in Figure 12. The shape of a corrugated deck plate attached to the bottom of the slab is not modeled directly. Rather, it is modeled as a flat plate with a gap, as shown in Figure 9(c). The width of the gap is determined by considering the depth of the troughs on the corrugated deck plate. The slab and flanges of beams are connected to the gap by studs, which are modeled by rigid beam elements. The slabs for the roof floor are directly connected to beams by consistently sharing nodes. Table 4 shows the number of rigid beam elements for modeling the studs. A wire mesh of steel bars of 6 mm in diameter in the slab is modeled by solid elements, as shown in Figure 9(c). The wire mesh is reinforcement for crack-width control. The circular cross section of these bars is approximately modeled as a square. The Young's modulus of the bars is changed in order to consider the difference in the area of the cross section of the square and that of the circle.

The column bases are also modeled using solid elements, as shown in Figure 9(d). The anchor bolts and seamless pipes that reinforce the H-shaped steel members of the base are modeled by truss elements. Each end of the truss element is connected to a number of nodes around the truss using a set of rigid beam elements. An initial tension of 100 kN is imposed in each anchor bolt. The contact conditions between the base plate, the mortar, and the base are not considered. Rather, they are modeled as a unified mesh, i.e., the nodes on the material boundary are shared by meshes with different material properties.

The exterior walls, which are made of ALC (Autoclaved Lightweight aerated Concrete) panels, are modeled by elastic-plastic shear springs. The nonlinear springs are introduced in order to consider the effect of hysteretic damping due to the plastic and frictional energy dissipation in the exterior wall. These springs represent both the frictional contact behavior between the walls and the nonlinear material property of the ALC panel. The parameters are determined based on the experimental results [38]. In the present analysis model, the Rayleigh damping is also introduced as described in Section 4.1.

The piecewise-linear combined isotropic-kinematic hardening model, which was described in Section 2.2, is used for steel, and its parameters are determined from the results of the uniaxial tests under monotonic loading distributed for the blind analysis contest [27], and from the results of the uniaxial tests under cyclic loading conducted by Yamada et al. [39]. Note that no cyclic material test was conducted for the E-Defense test. The tests in Ref. [39] were conducted for the same type of steel materials as those used in the four-story frame. The monotonic uniaxial tests were conducted for all of the members. Therefore, different stress-strain curves are used for different members. The number of parameters for the hardening model is 18. Seven parameters, including the three parameters in Table 5, have fixed values, and the values of the other 11 parameters are identified using an optimization technique.

The following extended Drucker-Prager yield criterion is introduced for the concrete material used in the slabs:

$$F = \sqrt{l_0^{\,2} + q^2} - p\tan\beta - d' = 0 \tag{3}$$

where q is the equivalent stress, p is the hydrostatic stress, β is the internal frictional angle, and l_0 and d' are the parameters used to determine the shape of the yield function. The parameter l_0 represents the sharpness of the hyperbolic curve. The material properties are

summarized in Table 6. The compressive and tensile strengths are considered to be given by the yield stress. If the shear strength is assumed to be 1/8 the compressive strength and is also given by the yield stress, the value of l_0^2 is calculated to be a negative value. Therefore, the value of l_0 is assumed to be 3.0, and the shear strength given by the yield stress is calculated based on this value.

The self-weight of the steel is computed based on a mass density of 7.86×10^{-6} kg/mm^3. In contrast, the mass density of 2.3×10^{-6} kg/mm^3 of the slab is increased appropriately to include the mass of nonstructural components, anti-collapse frames, and stair landings installed in the experimental model.

4. Results of numerical simulations

In this section, the eigenvalue analysis and the seismic response analyses under the 60%, 100%, and 115% excitations of the JR Takatori record (hereinafter, the 60%, 100%, and 115% Takatori waves) of the 1995 Hyogoken-Nanbu earthquake are performed using E-Simulator, and the results are compared with those obtained by the E-Defense full-scale shake-table test. The mesh described in Section 3.2 is used. Note that the same incompatible element [35][36] that was used in the buckling analyses in Section 3.1 is used. In the following analyses, the initial and maximum time increments are taken to be 0.01 s, and the minimum time increment is taken to be 1.0×10^{-6} s. The time increment is set automatically in the solver, i.e., the time increment is normally the maximum value, 0.01 s, and becomes smaller when the Newton-Raphson method does not converge.

4.1 Eigenvalue analysis and coefficients for the Rayleigh damping

The five lowest natural periods for the analysis model are listed in Table 7. The experimentally obtained natural periods for the first and second modes are also shown in Table 7. The analytical results agree well with the experimentally obtained values. The Rayleigh damping is applied in the following analyses. The coefficients for the Rayleigh damping are calculated using damping factors of 0.021 and 0.019 for the first and fourth modes, respectively, which are obtained by the eigenvalue analysis. These modes are the two lowest eigenmodes in the X-direction. The tangent stiffness matrix under the assumption that all materials are elastic is used for the calculation of the damping matrix. The coefficient α for the mass matrix and the coefficient β for the elastic tangent stiffness matrix are calculated to be 0.251 and 0.00118(0.118 in published version is mistake!), respectively.

4.2 Seismic response analyses under the 60% Takatori wave

First, the static analysis for the application of self-weight is conducted, and then the seismic response analysis is performed. Large strain elastoplasticity is considered in the analyses. A 20-second segment of the 60% Takatori wave was used as an input ground motion for the E-Defense test. The acceleration measured on the shaking table during the test [40] is imposed on the bottom of the foundation in the analysis using E-Simulator. The NS, EW, and UD components are input for the *Y*-, *X*-, and *Z*-directions, respectively. The computation time using 256 cores (one node) of the SGI Altix 4700 supercomputer (CPU: 1.66-GHz dual core Intel Itanium processor, 256-core/node, eight nodes) is approximately one month. The total number of time steps is 5,020. The automatic time increment is used. The average computation time for one time step, including the nonlinear iterative steps for the Newton-Raphson method, is approximately 1,592 s. Note that the average computation time is obtained from the computation time for the first 24 time steps. When 360 nodes (2,880 cores) of the K computer [41] are used, the average computation time is 556 s.

Figures 13(a) through 13(d) and 14(a) through 14(d) show the time histories of the interstory drift angle and the story shear force of the first story (base shear), respectively, which are obtained by the analysis using E-Simulator and the E-Defense test [25][26]. For E-Simulator, the results obtained using the combined hardening model for the steel material and those obtained using the isotropic hardening model are shown. The interstory drift angle is calculated from the lateral displacements at the center of the second floor. The shear force is calculated as the summation of the total mass of each floor multiplied by the acceleration at the center of gravity of each floor.

The interstory drift angle along the *X*-axis obtained by E-Simulator, as shown in Figure 13(a), agrees well with the experimental results until approximately 7 s. However, the differences in the phase and amplitude become larger after 7 s, at which point the amplitude of the input ground motion decreases. In addition, the difference between the results obtained using the combined hardening model and those obtained using the isotropic hardening model is small. The interstory drift angle along the *Y*-axis obtained by E-Simulator, as shown in Figure 13(b), is in good agreement with the experimental results when the combined hardening model is used. On the other hand, the interstory drift angle remains in the positive region in the latter part of the time history when the isotropic hardening model is used. Note, however, that Isobe et al. reported that this constant angle drift of the interstory drift angle in the *Y*-direction did not appear in their analysis using a beam model even when the isotropic hardening was assumed [20]. This indicates that the validation of a numerical code should be conducted from several viewpoints.

The time histories of the shear force in Figures 14(a) through 14(d) obtained by E-Simulator and E-Defense agree very well. In the *X*-direction (Figures 14(a) and 14(c)), however, the time histories appear to show similar tendencies to those of the interstory drift angle in Figure 13(a), i.e., the differences in the phase and in the amplitude become larger after 7 s. For the shear force, the difference between the results obtained using the combined hardening model and those obtained using the isotropic hardening model is small in both the *X*- and *Y*-directions.

Figure 15 shows the deformation and the distribution of the equivalent stresses at 6.08 s. The deformation is magnified 10 times, and the colors represent the distribution of the equivalent stresses. A torsional deformation is identified in the analysis results, but is not clearly observed in the E-Defense test. One reason for this discrepancy may be that the stiffness of the shear spring used in the E-Simulator model to represent the exterior walls does not take into account the degradation in stiffness and strength due to local fracture.

4.3 Seismic response analyses under the 100% and 115% Takatori waves

The acceleration measured on the shaking table during the test under the excitation of the Takatori record (100% Takatori wave) [40] is imposed on the bottom of the foundation in the analysis using E-Simulator. The E-Defense tests were conducted using the same specimen with the input waves with gradually increasing in scale factors, i.e., the 5%, 10%, 12.5%, 20%, 40%, 60%, and 100% Takatori waves [25][26]. The elastic-plastic responses were observed in the cases of the 40%, 60%, and 100% Takatori waves. Therefore, plastic deformation due to the preceding tests remains in the specimen before the test using the 100% Takatori wave. In the simulation using E-Simulator, however, the initial plastic deformation is not considered due to the limitation of computer resources. In the E-Defense test, the frame fully collapsed under the 100% Takatori wave, and complete collapse was stopped by the anti-collapse frames. In the simulation using E-Simulator, however, the frame does not fully collapse under the 100% Takatori wave. Therefore, simulations under the 115% Takatori wave are also performed. Note that the 115% Takatori wave is generated by multiplying the data of the

100% Takatori wave by 1.15. First, the static analysis for the application of self-weight is conducted, and then the seismic response analysis is performed. Large strain elastoplasticity is considered. The combined hardening model for the steel material is used.

An important phenomenon in the response under the 100% Takatori wave is that the contact between the column and the slab occurs as described in Section 3.2. Figures 16(a) and 16(b) show the deformations obtained by the model with the separate condition and the model with the stick condition, respectively. The deformation due to buckling at the upper part of the column is observed for the model with the stick condition (Figure 16(b)), but is not observed for the model with the separate condition (Figure 16(a)). Note also that the model with the separate condition is used in the simulation for the 60% Takatori wave described in the previous section, i.e., the separate model performs better than the stick model before the local buckling and the collapse of the entire frame occurs. Note that the introduction of the contact condition is important in order to achieve a more accurate reproduction of the test. However, this is a topic for future research.

Figures 17(a) through 17(d) show the time histories of the interstory drift angle obtained by E-Simulator and the E-Defense test. The frame collapsed completely in the positive *X*- and *Y*-directions after 6 s in the test, as shown in Figure 19(a), and the collapse was suppressed by the anti-collapse frames [25]. Figures 17(c) and 17(d) show the time histories of the interstory drift angle magnified for the interval between 2 and 6 s. The magnitude of the drift angle is smaller than the experimental result, even for the case under the 115% wave. In the *X*-direction, the difference between the results obtained by the model with the separate condition and the model with the stick condition is small, although some differences are observed in the *Y*-direction.

Figures 18(a) through 18(d) show the time histories of the shear force of the first story obtained by E-Simulator and the E-Defense test. The results are in good agreement. In the elastic region between 0 s and 2 s, the response obtained by E-Simulator for the 115% wave is larger than that for the 100% record. However, the difference in the responses for the 100% and 115% waves are small in the plastic region after 2 s. The response for the 115% wave is sometimes smaller than that for the 100% record. This phenomenon may be due to the larger dissipation of plastic energy in the 115% wave case. Figures 18(c) and 18(d) show the time histories of the shear force magnified for the interval between 3.6 and 6.8 s. Before the collapse occurs, i.e., before the buckling occurs, the results obtained by the model with the separate condition agree better with the experimental results than with the results obtained by the model with the stick condition.

Figures 19(a) and 19(b) show the global and local deformations, respectively, in the collapsed state in the E-Defense test under the 100% Takatori wave [40]. Figures 20(a) and 20(b) show the deformation and distribution of the equivalent stress at 6.36 s simulated by E-Simulator using the model with the stick condition under the 115% Takatori wave. The collapse behavior of the entire frame is simulated successfully. The deformation due to the local buckling found in Figure 19(b) is simulated well, as shown in Figure 20(b). Note, however, that the reverse deformation mode is observed in the simulation results, although the same inextensible buckling mode is obtained. Figures 21(a) and 21(b) show the deformation and the distribution of the equivalent stresses at 6.46 s in the *YZ*- and *ZX*-planes, respectively. The deformation is not magnified, and the colors represent the distribution of the equivalent stresses. The collapse of the first story in the *Y*-direction is clearly observed. The deformed shape is different from that in the 60% Takatori case. Figures 22(a) and 22(b) show the distribution of the equivalent stress in the concrete used in the second floor slab and in steel bars, respectively. The stress concentration around a column at the position at which the contact between the slab and the column occurs is observed. Stress concentration is also

observed around the steel bars, which do not yield.

4.4 Discussion of the analysis model

The approximations assumed in the present analysis model are summarized as follows: (1) the contact between the base plate, mortar, and base, and the contact between a column and a slab are not introduced; (2) the nonlinear behaviors of anchor bolts and seamless pipes in the column base are not taken into account; (3) the plastic deformation and residual stress due to manufacturing and welding processes and the preceding input ground motions are not taken into account; (4) the degradation in stiffness and strength due to local fracture is not considered in the shear springs that represent the exterior wall; (5) the shape of a corrugated deck plate attached to the bottom of the slab is not modeled; and (6) the extended Drucker-Prager yield criterion is not sufficient for modeling the concrete.

The collapse of the frame under the 100% Takatori wave may be reproduced by improving the analysis model with respect to the above items. Accurate modeling of the hysteretic damping due to the plastic and frictional energy dissipation contributes to improving the response. Therefore, item (4) may also affect the results for the 60% Takatori wave. Although the contact model must be introduced in order to overcome item (1), its computation cost in the dynamic analysis is very high because a sufficiently small time increment is required in order to capture impact phenomena and to perform a stable numerical computation.

5. Concluding remarks

Dynamic collapse analyses of the four-story steel building, for which a full-scale shake-table test was conducted at E-Defense, are performed using E-Simulator, which is a parallel finite element analysis software package for civil and building structures. The frame is modeled by solid elements. The elastic-plastic buckling analyses of a column are conducted using meshes of various mesh densities for the code verification and the calculation verification of the analysis model. The mesh density of each part of the mesh of the four-story frame is then determined.

In the analysis under the 60% Takatori wave, the time histories of the interstory drift angle and the story shear force obtained by E-Simulator show good agreement with the experimental results, especially when the combined hardening model proposed in Ref. [32] is used. Accurate modeling of the hysteretic damping due to the plastic and frictional energy dissipation is necessary in order to improve the simulation.

In the analysis under the 100% and 115% Takatori waves, both the response of the entire frame and the local deformation due to plastic buckling are well simulated by E-Simulator. Since contact occurs between the column and slab, simulations using the models with and without the stick condition are performed. The results of the simulation using the model with the stick condition indicate that the contact phenomenon induces buckling at the upper part of the column of the first story. The introduction of the contact condition will be a topic of future study.

The present study demonstrates that precise modeling of local phenomena such as inelastic material modeling and geometry modeling improves the reproduction of global responses, such as collapse. In this modeling strategy, only simple material tests are required in order to obtain the parameters for the analysis model. The present study demonstrates the feasibility of a large-scale structural analysis in the field of earthquake engineering and is novel from the viewpoint of the computational mechanics. Few studies have achieved large-scale highly nonlinear finite element structural analysis using a mesh with approximately 20 million degrees of freedom, even in other fields, such as mechanical

engineering.

ACKNOWLEDGEMENTS
The present study is part of the E-Defense Seismic Experimental Research and Simulation System Construction Project conducted by the E-Simulator Development Committee (Leader: Prof. Muneo Hori, The University of Tokyo) at NIED. The authors acknowledge the valuable contributions of Dr. Hiroyuki Tagawa (NIED), Prof. Masayuki Kohiyama (Keio University), and the other members of the committee, as well as the financial support of NIED. The contributions of Dr. Tomonobu Ohyama and Mr. Kiyoshi Yuyama (Allied Engineering Corporation) to code development, computation, and mesh generation are also acknowledged. The present study was also supported by JSPS KAKENHI (grant number 24560080) and by MEXT through a grant for research on HPCI Strategic Program Field No. 3.

REFERENCES
[1] Ohtani K, Ogawa N, Katayama T, Shibata H. Construction of E-Defense (3-D Full-Scale Earthquake Testing Facility). In: Proceedings of the 13th World Conference on Earthquake Engineering; 2004, Vancouver, B.C., Canada.
[2] Website of Hyogo Earthquake Engineering Research Center (E-Defense) of the National Research Institute for Earth Science and Disaster Prevention (NIED), http: //www.bosai.go.jp/hyogo/ehyogo/index.html.
[3] Hori M, Noguchi H, Ine T. Project Report of Development of Numerical Shaking Table Coping with E-Defense. JSCE J Earthquake Eng 2007; 29: 1420-1425, [in Japanese].
[4] Website of Allied Engineering Corporation, http: //www.alde.co.jp/english/index.html.
[5] Suzuki M, Ohyama T, Akiba H, Yoshimura S, Noguchi H. Development of Fast and Robust Parallel CGCG Solver for Large Scale Finite Element Analyses. Transactions of the Japan Society of Mechanical Engineers 2002: A68, 1010-1017 (in Japanese).
[6] Akiba H, *et al*. Large Scale Drop Impact Analysis of Mobile Phone Using ADVC on Blue Gene/L. In: Proceedings of the International Conference on High Performance Computing Networking and Storage (SC06) 2006, Tampa, USA.
[7] Akiba H, Ohyama T, Shibata Y. CGCG Method for Structural Analysis and Its Enhancement, In: Proceedings of ECT2010, Valencia, 14-17 September, 2010.
[8] Website of ADVENTURE project, http: //adventure.sys.t.u-tokyo.ac.jp/.
[9] Yoshimura S, Shioya R, Noguchi H, Miyamura T. Advanced General-Purpose Computational Mechanics System for Large Scale Analysis and Design. J Comput Appl Math 2002; 149: 279-296.
[10] Ohsaki M, Miyamura T, Kohiyama M, Noguchi H, Akiba H, Hori M, Kajiwara K, Ine T. High-Precision Finite Element Analysis of Elastoplastic Dynamic Responses of Super-Highrise Steel Frames. Earthquake Engng Struct Dyn 2009; 38: 635-654.
[11] Miyamura T, Ohsaki M, Kohiyama M, Isobe D, Onda K, Akiba H, Hori M, Kajiwara K, Ine T. Large-Scale FE Analysis of Steel Building Frames Using E-Simulator. Prog Nucl Sci Tech 2011; 2: 651-656.
[12] Ribakov Y, Gluck J, Reinhorn AM. Active Viscous Damping System for Control of MDOF Structures. Earthquake Engng Struct Dyn 2001; 30: 195-212.
[13] Nakashima M, Ogawa K, Inoue K. Generic Frame Model for Simulation of Earthquake Responses of Steel Moment Frames. Earthquake Engng Struct Dyn 2002; 31(3): 671-692.
[14] Ibarra LF, Medina RA, Krawinkler H. Hysteretic Models that Incorporate Strength and Stiffness Deterioration. Earthquake Engng Struct Dyn 2005; 34(12): 1489-1511.
[15] Lignos, DG, Krawinkler H, Whittaker AS. Prediction and Validation of Sidesway

Collapse of Two Scale Models of a 4-Story Steel Moment Frame. Earthquake Engng Struct Dyn 2011; 40(7): 807-825.

[16] Wang T, McCormick J, Yoshitake N, Pan P, Murata Y, Nakashima M. Collapse Simulation of a Four-Story Steel Moment Frame by a Distributed Online Hybrid Test, Earthquake Engng Struct Dyn 2008; 37(6): 955-974.

[17] Tada M, Tamai H, Ohgami K, Kuwahara S, Horimoto A. Analytical Simulation Utilizing Collaborative Structural Analysis System. In: Proceedings of the 14th World Conference on Earthquake Engineering (14WCEE) 2008, Beijing, China.

[18] Horimoto A, Tada M, Tamai H, Ohgami K, Kuwahara S, Mitani A. Three Dimensional Analytical Simulation of Collapse by Collaborative Structural Analysis for Full-Scale 4-Story Steel Building. Journal of structural engineering. B 2009 (Architectural Inst. of Japan); 55B: 277-283 [in Japanese].

[19] Nam TT, Kasai K. Dynamic Analysis of a Full-Scale Four-Story Steel Building Experimented to Collapse Using Strong Ground Motions, In: Proc. Int. Symp. Disaster Simulation and Structural Safety in the Next Generation 2011 (DS'11); 2011: 311-318, Kobe, Japan.

[20] Isobe, D, Han, WS, Miyamura, T. Verification and validation of a seismic response analysis code for framed structures using the ASI-Gauss technique. Earthquake Engng Struct Dyn 2013; 42(12): 1767-1784.

[21] Lynn KM, Isobe D. Finite Element Code for Impact Collapse Problems of Framed Structures. Int J Numer Meth Eng 2007; 69(12): 2538-2563.

[22] Krishnan S. Modified Elastofiber Element for Steel Slender Column and Brace Modeling. J Struct Eng 2010; 136(11): 1350–1366.

[23] Jin J, El-Tawil S. Inelastic Cyclic Model for Steel Braces. J Eng Mech 2003; 129(5): 548–557.

[24] Mizushima Y, Mukai Y, Ohno M, Saruwatari T, A Study on Strong Non-Linearity Analysis with Large-Scale and Detailed FE Models -Comparison of Dynamic Responses of Frame and Lumped Mass Models-. In: Proceedings of International Symposium on Earthquake Engineering, Japan Association for Earthquake Engineering (JAEE); 2012; 1: 517-524.

[25] Yamada S, Suita K, Tada M, Kasai K, Matsuoka Y, Shimada Y. Collapse Experiment on 4-Story Steel Moment Frame: Part 1 Outline of Test Results. In: Proceedings of the 14th World Conference on Earthquake Engineering (14WCEE); 2008, Beijing, China.

[26] Suita K, Yamada S, Tada M, Kasai K, Matsuoka Y, Shimada Y. Collapse Experiment on 4-Story Steel Moment Frame: Part 2 Detail of Collapse Behavior. In: Proceedings of the 14th World Conference on Earthquake Engineering (14WCEE); 2008, Beijing, China.

[27] Ohsaki M, Kasai K, Matsuoka Y, Zhang JY. Results of Recent E-Defense Tests on Full-Scale Steel Building: Part 2, Collapse Simulation and Blind Analysis Contest. In: Proceedings of the Structures Congress; 2008, ASCE, Vancouver.

[28] Mandel J. Balancing domain decomposition. Comm Numer Meth Eng 1993; 9: 233-241.

[29] Yagawa G, Shioya R. Parallel Finite Elements on a Massively Parallel Computer with Domain Decomposition. Computing Systems in Engineering 1993; 4: 495-503.

[30] Miyamura T, Yoshimura S. Generalized I/O Data Format and Interface Library for Module-Based Parallel Finite Element Analysis System. Advances in Engineering Software 2004; 35: 149-159.

[31] Hughes TJR. The finite element method - Linear static and dynamic finite element analysis. Dover publications, 2000: 532-551.

[32] Ohsaki M, Zhang JY, Miyamura T. A Heuristic Algorithm for Parameter Identification of

Steel Materials Under Asymmetric Cyclic Elastoplastic Deformation. In: Proc. 7th China-Japan-Korea Joint Symposium on Optimization of Structural and Mechanical Systems (CJK-OSM7); 2012, Huangshan, China, Paper No. J045.

[33] Miyamura T. Incorporation of Multipoint Constraints into the Balancing Domain Decomposition Method and Its Parallel Implementation. International Journal for Numerical Methods in Engineering 2007; 69: 326-346.

[34] Yamashita T, Miyamura T, Akiba H, Kajiwara K. Verification of Finite Element Elastic-Plastic Buckling Analysis of Square Steel Tube Column Using Solid Element, Transactions of the Japan Society for Computational Engineering and Science 2013; 2013: Paper No. 20130001 [in Japanese].

[35] Simo JC, Rifai MS. A Class of Assumed Strain Methods and the Method of Incompatible Modes, International Journal for Numerical Methods in Engineering 1990; 29: 1595-638.

[36] Simo JC, Armero F. Geometrically Nonlinear Enhanced Strain Mixed Methods and the Method of Incompatible Modes, International Journal for Numerical Methods in Engineering 1992; 33: 1413-1449.

[37] Yamada S, Satsukawa K, Kishiki S, Shimada Y, Matsuoka Y, Suita K. Elasto-Plastic Behavior of Panel Zone in Beam to External Column Connection with Concrete Slab, Journal of Structural and Construction Engineering (Transactions of Architectural Inst. of Japan), 2009; 74(644): 1841-1849 [in Japanese].

[38] Matsuoka Y, Matsumiya T, Suita K, Nakashima M. Test on seismic performance evaluation of exterior ALC walls with opening: E-Defense experimental projects for steel buildings - Part 14, In: Summaries of Technical papers of Annual Meeting Architectural Institute of Japan, C-1, 2007: 1081-1082 [in Japanese].

[39] Yamada S, Imaeda T, Okada K. Simple Hysteresis Model of Structural Steel Considering the Bauschinger Effect, Journal of Structural and Construction Engineering (Transactions of Architectural Inst. of Japan), 2002; 67(559): 225-232 [in Japanese].

[40] Website of ASEBI at E-Defense, NIED, Project: E-Defense tests on full-scale four-story steel building, https: //www.edgrid.jp/data/.

[41] Website of K Computer (RIKEN Advanced Institute for Computational Science), http: //www.aics.riken.jp/en/.

Table 1: Number of time steps for different models with different values of Δt .

Model	Δt (upper limit of time increment) (s)	Total number of time steps	Time when computation is terminated (s)
t2b12L80	0.01	625	6.21
t2b12L80	0.04	244	5.34
t2b48L320	0.01	603	4.81
t2b48L320	0.04	397	4.75

Table 2: Dimensions of the element used in the mesh of a column of the four-story frame and in the mesh of model *t2b48L320*. (unit: mm)

	Mesh of a column of the four-story frame	Mesh of model *t2b48L320*
Element height	12.5	11.745
Element width	15	5.875
Element thickness	4.5	4.5

Table 3: Evaluation results for the quality of the hexahedral mesh of the four-story frame.

Story	Aspect ratio of element	Min Edge length (mm)	Max Edge length (mm)

	Min.	Max.	Min.	Max.	Min.	Max.
RF	1.00	49.0	2.0	54.0	12.0	147.0
2F-4F	1.34	39.0	3.0	72.5	12.0	117.0

Table 4: Number of rigid beam elements in each floor.

Floor	X	Y	Sum.
4F	87 (29×3 lines)	96 (48 × 2 lines)	183
3F	87 (29×3 lines)	96 (48 × 2 lines)	183
2F	87 (29×3 lines)	96 (48 × 2 lines)	183
Total number of stud bolts			549
Total number of rigid beam elements (number of stud bolts ×4)			2,196

Table 5: Material properties of steel.

Young's modulus (kN/mm^2)	205.0
Poisson's ratio	0.3
Mass density (kg/mm^3)	7.86×10^{-6}

Table 6: Material properties of concrete (parameters for the extended Drucker-Prager yield criterion).

Young's modulus (kN/mm^2)	25.61
Compressive strength (N/mm^2)	25.10
Tensile strength (N/mm^2)	2.180
Shear strength (N/mm^2)	1.510
Poisson's ratio	0.2
Mass density (kg/mm^3) (dead load is included)	6.26×10^{-6}
β (deg.)	67.14
l_0 (N/mm^2)	3.0
d' (N/mm^2)	5.433
Hardening coefficient (kN/mm^2)	2.561×10^{-2}

Table 7: Five lowest natural periods for the analysis model and the experimental model (s).

Model	Natural period				
	1st	2nd	3rd	4th	5th
Analysis	0.8262	0.8081	0.5418	0.2660	0.2611
Experimental [25]	0.82	0.74-0.78	---	---	---

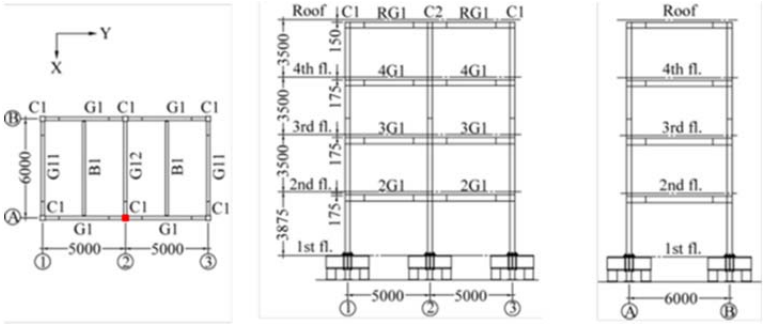

(a) Plan (first floor) (b) Y-elevation (c) X-elevation

Figure 1: Four-story steel frame [40] (unit: mm)

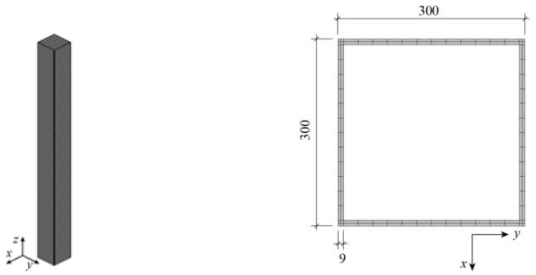

(a) Entire mesh (b) Cross section and sizes of the mesh (units: mm)

Figure 2: Analysis model ($t2b12L80$).

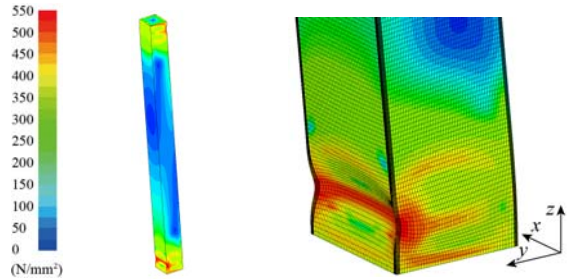

(a) Overall view (b) Close-up view

Figure 3: Deformation (not magnified) and contour plot of the equivalent stress for a prescribed displacement of 300 mm (model $t8b48L320$).

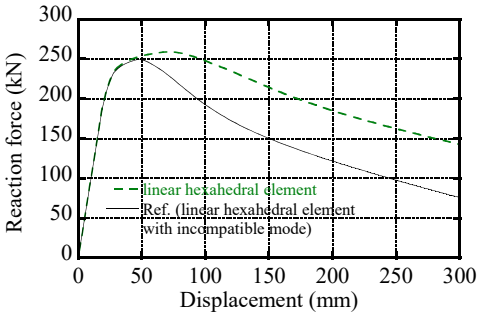

Figure 4: Relationship between the prescribed displacement and the reaction force for model $t8b48L320$ with linear hexahedral elements and linear hexahedral elements with the incompatible mode.

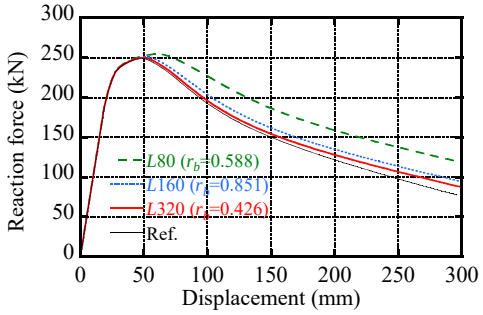

(a) Model $t4b12L\{80, 160, 320\}$

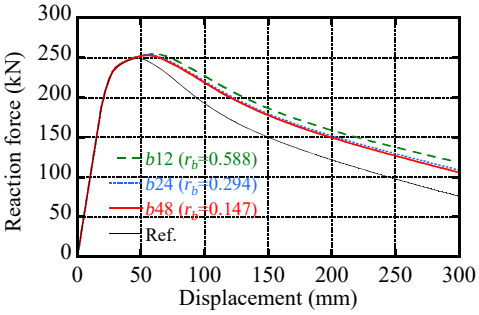

(b) Model $t4b\{12, 24, 48\}L80$

Figure 5: Relationship between prescribed displacement and reaction force for different numbers of mesh divisions in (a) the longitudinal direction and (b) the lateral directions.

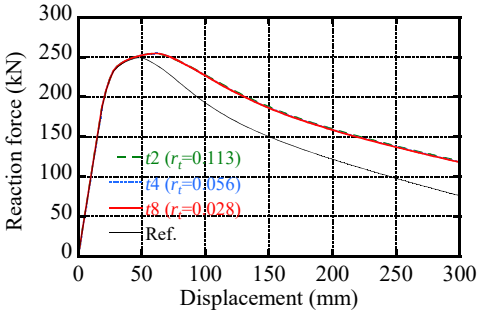

(a) Model $t\{2, 4, 8\}b12L80$ ($r_b = 0.588$)

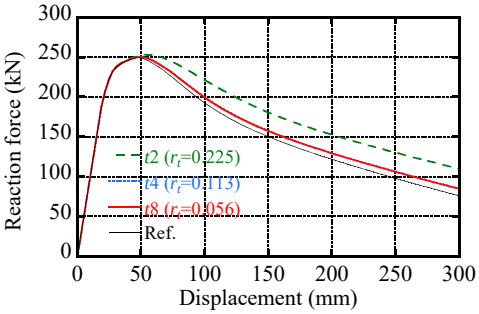

(b) Model $t\{2, 4, 8\}b24L160$ ($r_b = 0.588$)

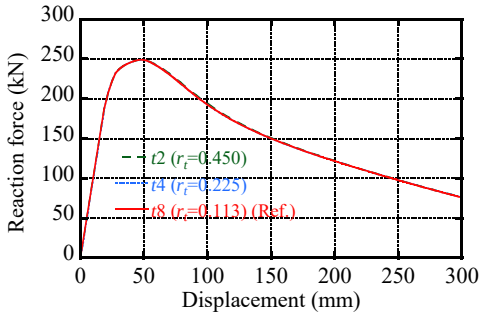

(c) Model $t\{2, 4, 8\}b48L320$ (r_b = 0.588)

Figure 6: Relationship between the prescribed displacement and the reaction force for different numbers of mesh divisions in the thickness direction.

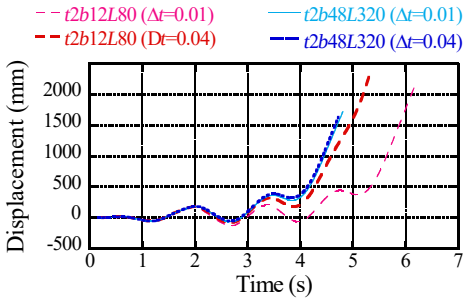

Figure 7: Time histories of displacement at the top of the column.

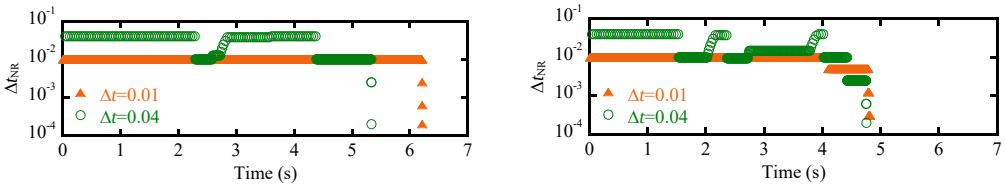

(a) $t2b12L80$ (b) $t2b48L320$

Figure 8: Time histories of Δt_{NR} .

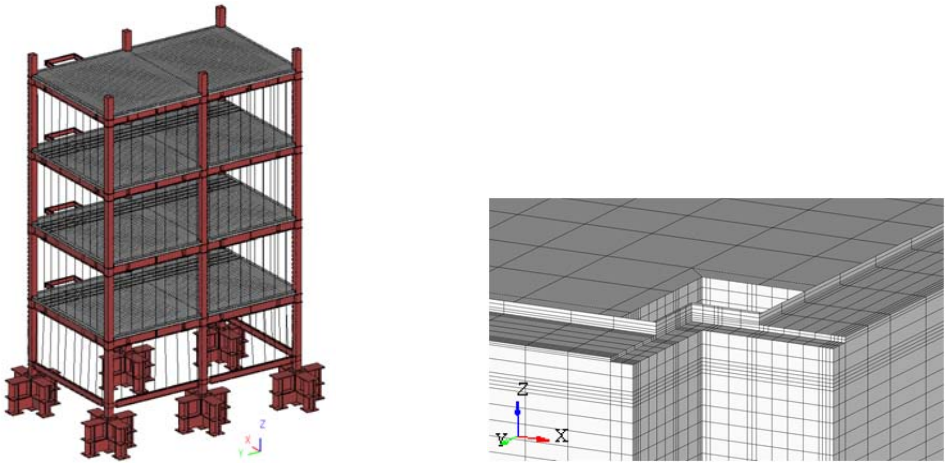

(a) Entire frame (b) Close-up view

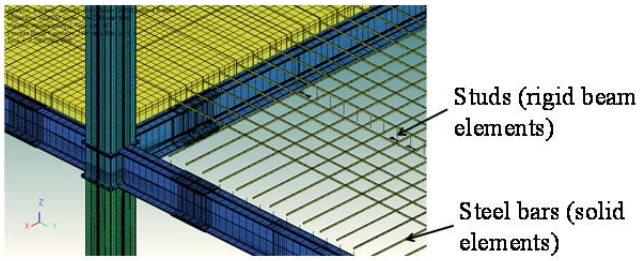

(c) Modeling of slabs, steel bars, and studs

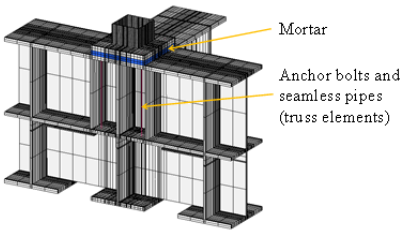

(d) Column base

Figure 9: Mesh of the four-story steel frame.

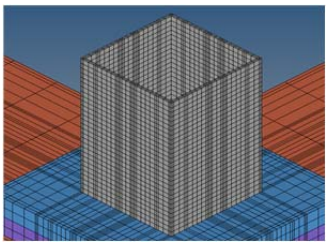

(a) Mesh of a column of the four-story frame

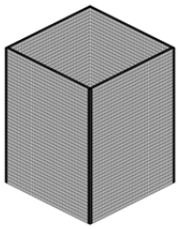

(b) Mesh of model *t2b48L320*

Figure 10: Comparison of mesh density between the mesh of a column and the mesh of model *t2b48L320*.

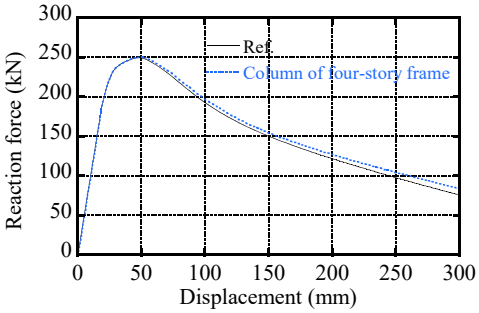

Figure 11: Relationships between the prescribed displacement and the reaction force for the column of the four-story frame and for model *t8b48L320*.

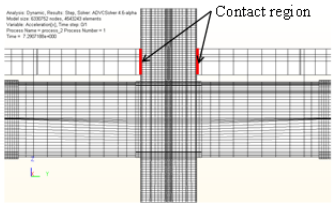

Figure 12: Region in which the contact between the column and the slab occurs.

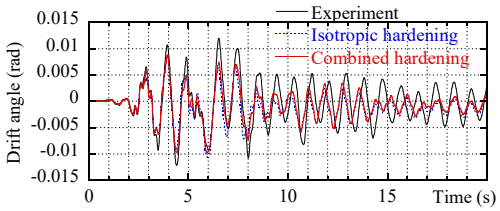

(a) X-direction

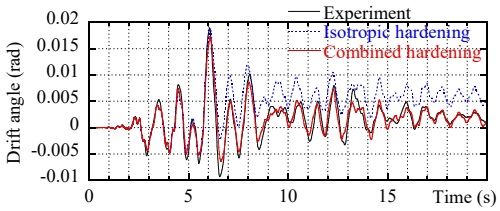

(b) Y-direction

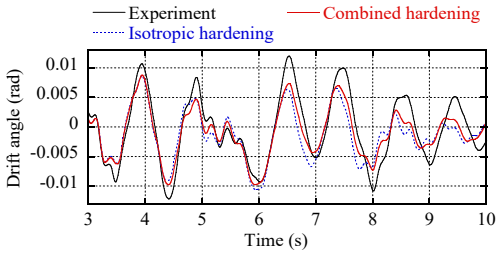

(c) X-direction (interval between 3 and 10 s)

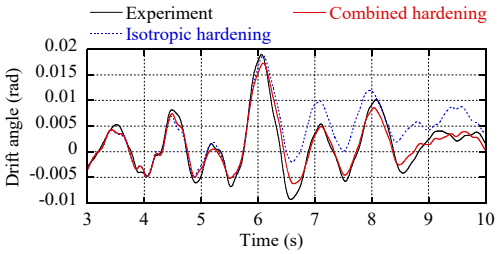

(d) Y-direction (interval between 3 and 10 s)

Figure 13: Time-histories of the interstory drift angle of the first story obtained by E-Simulator and

the E-Defense full-scale test.

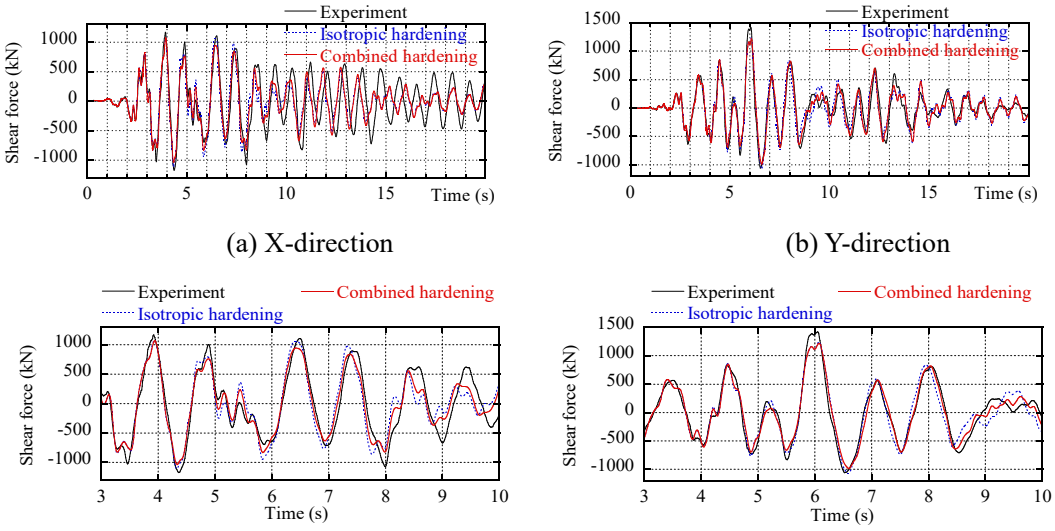

(a) X-direction (b) Y-direction

(c) X-direction (d) Y-direction

(interval between 3 and 10 s) (interval between 3 and 10 s)

Figure 14: Time-histories of the shear force of the first story obtained by E-Simulator and the E-Defense full-scale test.

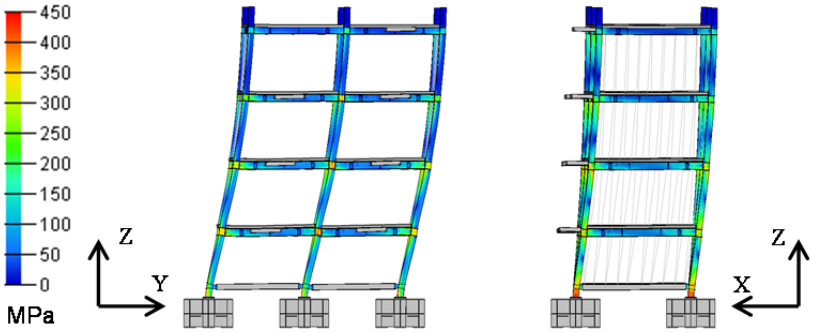

Figure 15: Deformation (magnified by a factor of 10) and distribution of the equivalent stress at 6.08 s obtained by E-Simulator.

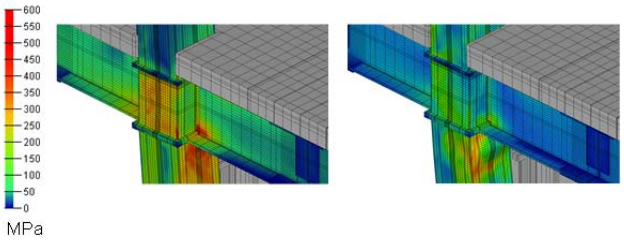

(a) Separate condition (b) Stick condition

Figure 16: Deformations around C2 column obtained by models with the separate condition and the stick condition under the 100% Takatori wave for (a) 6.24 s and (b) 6.29 s (maximum displacement is observed); deformation is not magnified; color contours indicate distributions of equivalent stress.

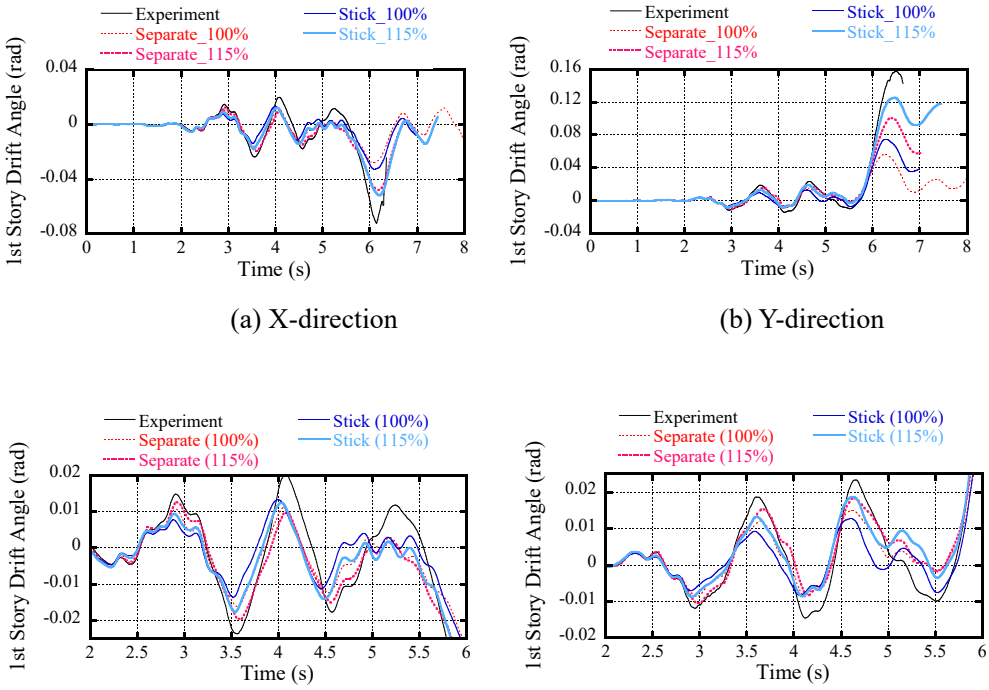

(a) X-direction (b) Y-direction

(c) X-direction (interval between 2 and 6 s) (d) Y-direction (interval between 2 and 6 s)

Figure 17: Time-histories of interstory drift angle of the first story obtained by E-Simulator and the E-Defense full-scale test.

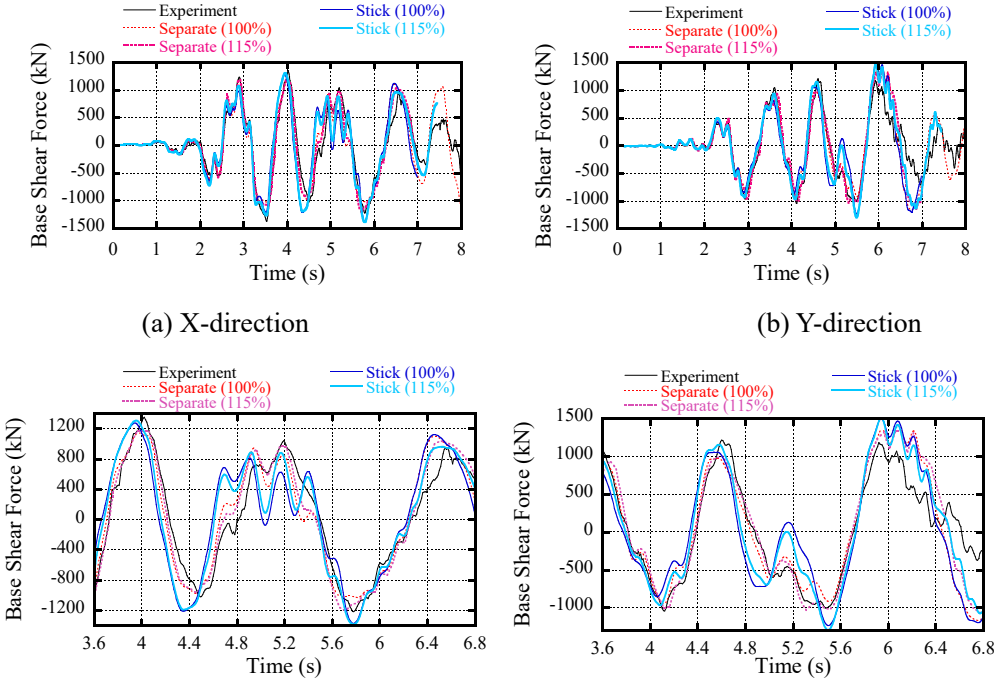

(a) X-direction (b) Y-direction

(c) X-direction (interval between 3.6 s and 6.8 s) (d) Y-direction (interval between 3.6 s and 6.8 s)

Figure 18: Time-histories of the shear force of the first story obtained by E-Simulator and the E-Defense full-scale test.

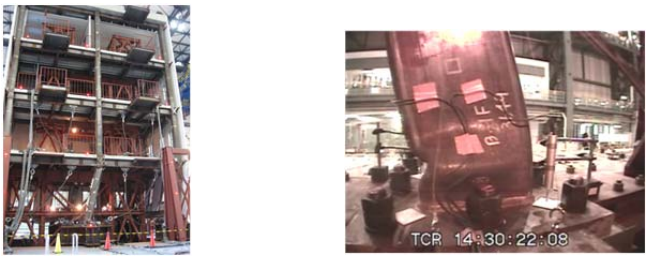

(a) Collapse of the entire structure (b) Local buckling in a column

Figure 19: Deformation in the collapsed state in the E-Defense full-scale test under the 100% Takatori wave [40].

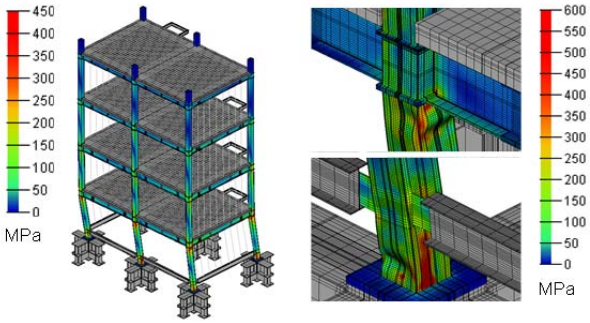

(a) Complete structure (b) Local buckling of a center column

Figure 20: Deformation (not magnified) and distribution of the equivalent stress at 6.46 s obtained by E-Simulator under the 115% Takatori wave (stick model). Note that the color bar is different from that in Fig. 16.

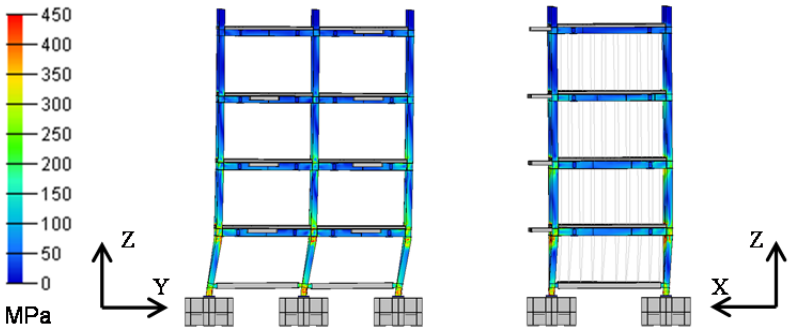

Figure 21: Deformation (not magnified) and distribution of the equivalent stress at 6.46 s obtained by E-Simulator.

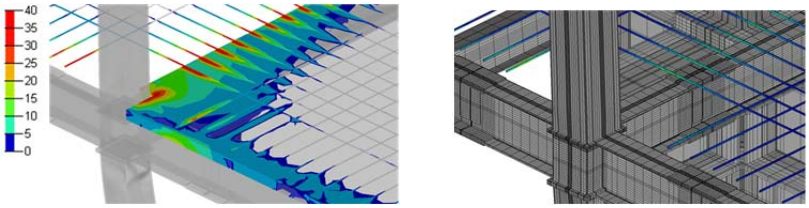

(a) Second floor slab (b) Steel bars

Figure 22: Distribution of the equivalent stress (a) in the second floor slab and (b) in steel bars at 6.46 s.